Available online at www.sciencedirect.com

ScienceDirect

IFAC PapersOnLine 56-2 (2023) 5352–5357

Model-based flux control of an electropermanent magnet for adaptive zero power gravity compensation

Alexander Pechhacker * **Daniel Wertjanz** * **Ernst Csencsics** * **Georg Schitter** *

* *Automation and Control Institute (ACIN), TU Wien, 1040 Vienna, Austria, Corresponding author: (e-mail: pechhacker@acin.tuwien.ac.at).*

Abstract: This paper presents a model-based flux control for a variable reluctance actuator with an electropermanent magnet, used for adaptive zero power gravity compensation in magnetic levitation systems. With the hysteresis of the electropermanent magnet being identified and approximated, tailored current pulses are applied by the model-based flux control to tune the magnetization of the electropermanent magnet. In this way, the resulting stationary reluctance force compensates the gravitational force of the levitated mover mass. Based on the identified hysteresis, a non-linear control law is derived, which is extended by an integrator term to compensate modelling uncertainties. In comparison to the state of the art model-free control, the model-based control increases the force tuning rate by a factor of 14 to 19 N/s and improves the robustness of the experimental system in variable mover positions.

Keywords: Mechatronics, Identification and control methods, Electromagnetics, Actuator, System identification, Hysteresis.

1. INTRODUCTION

Gravity compensation is required in many industrial applications ranging from conventional magnetic bearings [Yonnet (1981)] to magnetic suspensions [Golob and Tovornik (2003)], vibration isolation systems [Zhu et al. (2015)] and nanopositioning systems for the semiconductor industry [Yao et al. (2016); Zhang et al. (2014)].

Lorentz force-actuated systems are widely used to magnetically levitate masses with the drawback of a stationary coil current to compensate gravity [Wertjanz et al. (2020)]. A temperature increase, resulting from the power dissipation in the Lorentz coils, typically limits the precision of the entire system or makes cooling systems necessary [Hiemstra et al. (2014)]. Additionally, the stationary coil currents reduce the available force range of the Lorentz actuators for dynamic motions, limiting the performance of positioning or vibration isolation systems.

The attractive and repulsive forces of permanent magnets are utilized to passively compensate gravity by various system designs [Choi (2009); Hol et al. (2006); Deng (2017)]. These compensating forces are adapted for variable mover masses by changing the vertical position of the mover. A further design is based on a two degrees of freedom (DoFs) hybrid reluctance actuator, which uses the negative stiffness of the actuator to achieve a position-dependent compensation force [Stadler et al. (2022)]. Summing up, design approaches with permanent magnets are capable of zero power gravity compensation, but the vertical position needs to be adapted in relation to the mover mass. This problem can be solved by repositioning the permanent magnets with additional thermal shape memory actuators, resulting in variable compensation forces, which, however limit the force tuning rate of the gravity compensation to around $20\,\mathrm{mN/s}$ and reduce the power consumption only by a factor of 5 [Raab et al. (2021)].

In contrast to permanent magnets, electropermanent magnets (EPMs) are capable of adapting their magnetic flux via current pulses in an enveloping magnetization coil [Knaian (2010); Qin et al. (2020); Velez et al. (2018)]. An integrated electromagnetic actuator (IEA), combining a variable reluctance actuator with a seamlessly tunable EPM provides compensation forces between 0 and 25 N without static power consumption, while the mover is stabilized by integrated Lorentz actuators (LAs) [Pechhacker et al. (2022)]. This actuator design achieves a gravity compensation tuning rate of around $2.6\,\mathrm{N/s}$ and reduces the power consumption by four orders of magnitude.

Systems affected by hysteresis, such as electromagnetic actuators or piezo actuators caused by the material properties, are conventionally controlled by approaches based on the Prandtl-Ishlinskii model [Rakotondrabe (2012)], the Preisach model [Li et al. (2015)] or the Bouc-Wen model [Rakotondrabe (2011)]. To change the magnetization of EPMs, however high magnetic fields are required, which cannot be applied continuously due to the power dissipation [Knaian (2010)]. A model-free iterative control design, which linearly increases or decreases magnetic field pulses, adapts the compensating force of the IEA in a few seconds for a mass step [Pechhacker et al. (2022)]. For applications, such as positioning systems in arbitrary orientations for 3D measurements [Wertjanz et al. (2022)] or vibration isolation systems [Zhu et al. (2015)], the settling time for a changing mover mass or position limits the performance of

* The financial support by the Austrian Federal Ministry for Digital and Economic Affairs, and the National Foundation for Research, Technology and Development are gratefully acknowledged.

10.1016/j.ifacol.2023.10.180

those systems. Additionally, by reducing the settling time of the gravity compensation mechanism, the energy efficiency is further improved and the force tuning rate of the IEA is increased.

The contributions of this paper is a model-based flux control design for an adaptive gravity compensation with zero static power consumption and the experimental evaluation of the control performance regarding the force tuning rate.

2. INTEGRATED ELECTROMAGNETIC ACTUATOR

The core of the system concept is a variable reluctance actuator with a tunable permanent magnet, as shown in Fig. 1. By seamlessly tuning the magnetization of the EPM with current pulses applied to surrounding magnetization coil, an adaptable magnetic flux $\Phi_{EPM}(t)$ between mover and stator is obtained. The change of the magnetic flux results in an adapted reluctance force $F_{EPM}(t)$. A force equilibrium $F_{EPM}(t) = F_G(t)$ for a desired mover position is reached by tuning the reluctance force according to the gravitational forces acting on the mover. A change of the mover mass or the mover position requires a retuning of the EPM to maintain the force equilibrium.

The EPM is separated in a semi-hardmagnetic AlNiCo and a hardmagnetic NdFeB material with equal remanences and cross-sections. If both materials are magnetized in the same direction, the magnetic fluxes add up and the maximum flux (on state) is provided across the air gaps between stator and mover. If the AlNiCo material is magnetized in the anti-parallel direction to the NdFeB material, the magnetic flux of the NdFeB magnet is guided through the AlNiCo magnet inside the EPM and no external flux across the air gaps $\Phi_{EPM} = 0\,\mathrm{Wb}$ (off state) is generated by the EPM.

The force equilibrium position of the mover is unstable due to the negative stiffness in both air gaps of the variable reluctance actuator [Schmidt et al. (2020)]. Therefore LAs are integrated at each air gap to stabilize the desired mover position $d(t)$ via feedback control, as shown in Fig. 1.

The system control is cascaded in the inner position control loop and the outer EPM control. The position control applies the required current $i_{LA}(t)$ to the LAs to force the mover into the desired position. For a constant mover mass and position, the Lorentz force and current is constant. This constant offset current is proportional to the deviation from the force equilibrium $F_{LA}(t) = F_G(t) - F_{EPM}(t)$. By using the Lorentz currents as input for the EPM control, the power consumption is minimized with magnetization current pulses until the force equilibrium $F_{EPM}(t) = F_G(t)$ is reached and the currents in the LAs equal $i_{LA}(t) = 0$. The gravitational force of the mover mass is compensated and the mover is levitated with zero power consumption.

3. SYSTEM IMPLEMENTATION AND ANALYSIS

Figure 2 shows the cross-section of the actuator design, which combines a variable reluctance actuator with an EPM and two LAs at each air gap. The EPM consists of the cylindrical AlNiCo and NdFeB magnet, which have a diameter of $d_m = 10\,\mathrm{mm}$ and a length of $l_m = 30\,\mathrm{mm}$. The magnetization coil envelops the AlNiCo magnet with $N_{EPM} = 450$ turns, being a good design trade-off between low resistance as well as sufficiently high inductance to enable the tuning of the EPM. The mover position is defined by the air gap lengths d_1 and d_2,

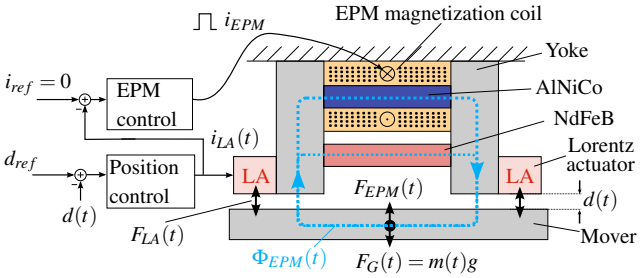

Fig. 1. System concept of the actuator. The EPM generates a flux $\Phi_{EPM}(t)$, which is adapted by the EPM controller to compensate the gravitational force $F_G(t)$ of the mover. The position control stabilize the mover position $d(t)$ with via the Lorentz coil currents $i_{LA}(t)$.

which are combined to $\boldsymbol{d} = [d_1 \quad d_2]^T$. Both stator yokes have a cross-section of $A_l = 20 \times 20\,\mathrm{mm}^2$. The described variable reluctance actuator with the EPM provides a seamlessly tunable reluctance force up to 25 N [Pechhacker et al. (2022)].

The integrated LAs provide a force in two DoFs with a motor-constant of $k_m = 9.65\,\mathrm{N/s}$, which are utilized to maintain the mover in the desired mover postion. A SISO position controller for each DoF stabilizes the mover in the desired position with a control bandwidth of 100 Hz for a load of 1 kg. The position control design ensures stability independent of the tunable EPM force.

As rapid prototyping system, an industrial EtherCAT bus coupler (EK1100, Beckhoff Automation GmbH & Co. KG, Germany) with several analog and digital I/O-cards is used to control the actuator prototype and to acquire the measurement data. The TwinCAT3 development tools enable the real-time position and EPM control with a Matlab/Simulink model. A sample frequency of 40 kHz is set and a time delay of $\tau_d = 100\,\mu\mathrm{s}$ is identified.

A common approach to change the magnetization of the permanent magnets are capacitive discharge magnetizers [Chen et al. (2003)]. Therefore, capacitors are charged to the voltage of 100 V and an IGBT full-bridge applies current pulses to the magnetization coil in the required direction. To avoid the time delay of the rapid prototyping system for accurate current pulses with a certain peak value, an analogue circuit controls the full-bridge and disconnects the charged capacitors from the magnetization coil when the reference peak current from the EPM control is reached.

3.1 EPM hysteresis

The B/H curve is characterized to identify the outer magnetic hysteresis behaviour for the subsequent model-based flux control design. The magnetic flux density B_l is measured at a displacement of $d_1 = d_2 = 1\,\mathrm{mm}$ in the center of the air gap with a Gauss-meter (GM08, Hirst Magnetics, UK) and a 0.6 mm transversal probe (TP002SP0.6, Hirst Magnetics, UK). The magnetic field strength H_{EPM} is generated with current pulses in the magnetization coil i_{EPM}. Due to the limited bandwidth of the Gauss-meter, the power dissipation in the magnetization coil and the thermal limits of actuator prototype, the B/H curve is identified based on the stationary magnetic flux density $B_{l,s}$, resulting from a current pulse with a certain peak value $\hat{i}_{EPM}$. Assuming a relative permeability of vacuum μ_0 in the recoil

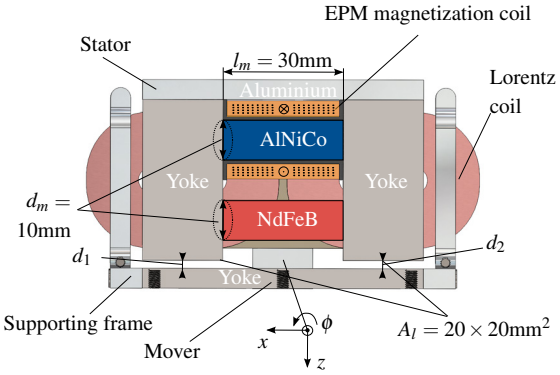

Fig. 2. Cross-section of the actuator design, consisting of the stator with the magnetization coil, the NdFeB and the AlNiCo magnet as well as the mover with the yoke for the EPM and the Lorentz coils.

lines, the magnetic flux of the EPM B_{EPM} can be linearly approximated by

$$B_{EPM} = B_{l,s}\frac{A_l}{2A_m} + \mu_0 H_{EPM}, \tag{1}$$

with the cross-section of the air gaps A_l and the EPM $2A_m$. As the magnetic field strength H_{EPM} cannot be measured, it is calculated using the peak values of the measured current pulses $\hat{i}_{EPM}$ by

$$H_{EPM} = \frac{N\hat{i}_{EPM} - \frac{B_{l,s}}{\mu_0}(d_1+d_2)}{l_m}\,. \tag{2}$$

The obtained B/H curve of the EPM is shown in Fig. 3 with the load-line specified as [Furlani (2001)]

$$B_{Load} = -\mu_0 \frac{A_l l_m}{2A_m(d_1+d_2)} H_{Load}\,, \tag{3}$$

and is shown for a mover position of $d_1 = d_2 = 1$ mm. The intersection points of the hysteresis and the load-line indicate the operating points of the EPM. Ideally, the lower curve should intersect the origin. An offset of 20 mT in P_{min} is measured, which is caused by a slightly higher remanence of the NdFeB in comparison to the AlNiCo magnet. Due to the load of the mover reluctance, the EPM is partially demagnetized in the stationary operating point and cannot provide the expected remanence of AlNiCo 5 $B_r \approx 1.25$ T [Campbell and Al-Murshid (1982)], resulting in a maximum flux density of 580 mT in P_{max}. By magnetizing or demagnetizing the EPM, the operating points along the load-line (e.g. P_1 or P_2) within the limits of the outer hysteresis can be obtained.

4. FLUX CONTROL DESIGN

In order to maintain the force equilibrium $F_{EPM}(t) = F_G(t)$ for a variable mover mass or position, the flux control tunes the magnetization of the EPM. The inner position control stabilizes the mover in the desired position with an offset force by each LA. The reluctance force of the EPM $F_{EPM}(t)$, the offset force $F_{off}(t)$ of each LA and the gravitational force $F_G(t)$ act on the mover and can be combined to

$$\underbrace{m(t)g}_{F_G(t)} = \underbrace{2k_m i_{off}(t)}_{F_{off}(t)} + F_{EPM}(t), \tag{4}$$

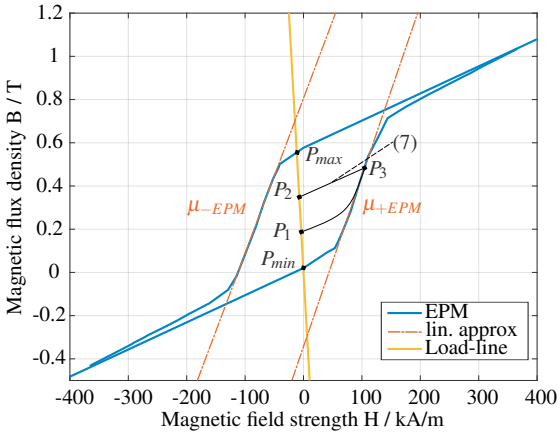

Fig. 3. Measured outer hysteresis of the EPM with the load-line for $d_1 = d_2 = 1$ mm.

with the motor constant of the LAs $k_m = 9.65\,\mathrm{N/A}$ and the mover mass $m(t)$. The offset force of the LAs is calculated by averaging the currents of both LAs, yielding $i_{off}(t)$. Additionally, a moving average filter with a window length of 4000 is used to implement a FIR low-pass filter, which attenuates high frequency disturbances caused by the positioning system. The input of the EPM control is the offset current $i_{off}(t)$ and the output is the peak current $\hat{i}_{EPM}$ to adapt the magnetization of the EPM. The accuracy of the flux control is limited by the disturbances coupled into the inner position control, such as friction, environmental vibrations, as well as the limited sampling time of the digital flux controller. Therefore, the EPM control is disabled, if the termination condition $|i_{off}| \leq 10$ mA is fulfilled [Pechhacker et al. (2022)].

4.1 Iterative control

A model-free iterative control is used as benchmark for the model-based control design, which is used to minimize the offset current $i_{off}(t)$ [Pechhacker et al. (2022)]. According to the sign of the offset current, the iterative control algorithm

$$I_{EPM} = \mathrm{sgn}(i_{off}(t))\Delta i_{EPM} \tag{5}$$

incrementally increases the peak value of the magnetization current pulses I_{EPM} using a step width of $\Delta i_{EPM} = 0.1$ A in the desired direction. Due to the limited inner position control bandwidth of 100 Hz, the sampling frequency of the iterative and model-based control are chosen to 10 Hz. If the termination condition is fulfilled, the control is disabled, but restarted if the threshold is exceeded again.

4.2 Model-based control

To increase the performance of the EPM tuning a model-based controller is designed based on the B/H curve of the EPM. The controller is synthesized by assuming a general operating point P_1 of the EPM with the magnetic flux density B_1, shown in Fig. 3, and an offset current in the LAs $i_{off,1}$ required to levitate the mover mass. In order to obtain the desired force equilibrium of the system, the reluctance force of the EPM needs to be increased by

$$\Delta F_{EPM} = (B_2^2 - B_1^2)\frac{(2A_m)^2}{A_l\mu_0} = 2k_m i_{off,1}, \tag{6}$$

with the permeability of vacuum μ_0, the cross-section of the stator yokes A_l and the EPM $2A_m$. By solving (6) for B_2 and by

calculating the corresponding field strength H_2 with the load-line (3), the operating point P_2 with zero power consumption is estimated. To calculate the unknown corner point P_3, the recoil-line between point P_2 and P_3 is linearly approximated by

$$B_{23} = \mu_0 H_{23} + B_{23,r}, \tag{7}$$

with the the permeability of vacuum μ_0 and the remanence $B_{23,r}$. The value of $B_{23,r}$ is determined with the operating point P_2 with B_2 and H_2. For reasons of simplicity and to reduce the number of parameters for the control law, the identified outer B/H curve is approximated by

$$B_{EPM} = \mu_{EPM} H_{EPM} + B_{EPM,r}\,. \tag{8}$$

According to the sign of $i_{off,1}$, the parameters μ_{EPM} and $B_{EPM,r}$ are defined for the positive and negative slope of the hysteresis, as shown for μ_{+EPM} and μ_{-EPM} in Fig. 3. The intersection of (8) and (7) yields the corner point P_3, which needs to be reached to stationary recoil to the desired zero power operating point P_2. The estimated magnetization current is calculated using the relation [Pechhacker et al. (2022)]

$$I_{EPM} = \frac{(d_1+d_2) l_m A_m (B_r \pm \mu_0 H_{Al} \pm B_{Al}) + H_{Al} l_m^2 A_l \mu_0}{N_{EPM} \mu_0 (A_l l_m + 2A_m (d_1+d_2))}\,, \tag{9}$$

with the length l_m, the remanence B_r and the cross-section A_m of the permanent magnets, the cross-section of the air gaps A_l and the number of turns of the magnetization coil N_{EPM}. The magnetic flux density B_{Al} and the field strength H_{Al} of the AlNiCo magnet is substituted by

$$H_{Al} = H_{EPM} \quad \text{and} \quad B_{Al} = 2B_{EPM} - \underbrace{(B_r + \mu_0 H_{EPM})}_{B_{NdFeB}}\,, \tag{10}$$

using Gauss' law. The magnetic flux of the EPM is the sum of the flux from the NdFeB B_{NdFeB} and AlNiCo magnet B_{Al}.

By combining (6) - (10), the control law $I_{EPM}(B_1, i_{off}, d_1, d_2)$ can be obtained, which estimates the required peak magnetization current to tune the EPM in relation to the magnetic flux density in the air gap B_1, the offset current in the LAs i_{off} and the mover position d_1 and d_2. To calibrate the linear approximation parameters of the hysteresis μ_{EPM} and $B_{EPM,r}$ for the rising (+) and falling curve (-), measurements are performed with magnetization current pulses applied to the initially switched off/on EPM (P_{min}/P_{max}), the resulting force is measured and the corresponding offset current i_{off} is determined at $d_1 = d_2 = 1\,\text{mm}$. The measurements are used to evaluate the hysteresis parameters ($\mu_{+EPM} = 1.6e-5$, $\mu_{-EPM} = 3e-5$, $B_{r,+EPM} = -0.6\,\text{T}$, $B_{r,-EPM} = 0.6\,\text{T}$), which are in the same order of magnitude as the identified hysteresis from Fig. 3. By comparing the calibration measurement data and the model-based control law for $d_1 = d_2 = 1\,\text{mm}$ in Fig. 4, deviations are observable for higher magnitudes of offset currents. These deviations are caused by the saturation of the EPM, resulting in a limited operating range of the EPM reluctance force, i.e. the offset force provided by LAs exceed the tuning range of the EPM reluctance force. However, these effects only occur with masses at the limits and above the specifications of the IEA and only minor modelling uncertainties are observable in the operating range of the EPM, yielding a suitable model for the control design.

To compensate unmodeled uncertainties, which may be caused by the hysteresis of the yokes, eddy currents or temperature dependencies, an integrator term is added to the control law

$$I_{EPM,I} = I_{EPM}(B_1, i_{off}, d_1, d_2) + k_I \int i_{off}(t)\,dt \tag{11}$$

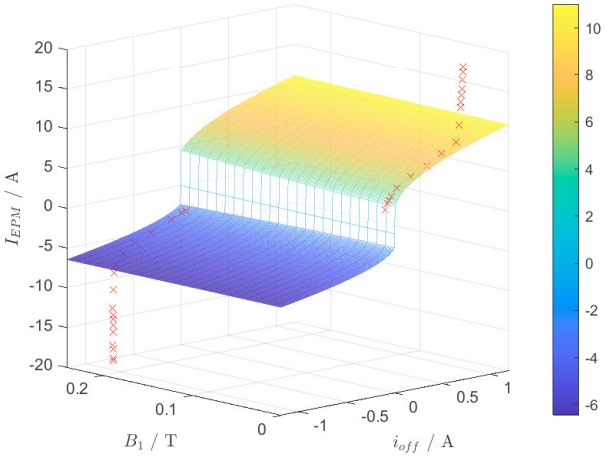

Fig. 4. Non-linear control law $I_{EPM}(B_1, i_{off}, d_1, d_2)$ with the calibration measurement marked in red $d_1 = d_2 = 1\,\text{mm}$.

with the integrator-gain k_I and the control error based on the offset current i_{off}. As the reluctance force tuning by I_{EPM} reveals a higher sensitivity for negative offset currents, an integrator state is introduced for each region according to the sign of i_{off}. The integrator-gains are experimentally tuned for $i_{off} > 0$ to $k_I = 150/\text{s}$ and for $i_{off} < 0$ to $k_I = 75/\text{s}$. Due to the higher magnetization currents required to increase the magnetic flux of the EPM ($i_{off} > 0$) in comparison to decrease it, as observable in Fig. 4, a higher integrator-gain for positive offset currents is chosen.

5. EVALUATION OF SYSTEM PERFORMANCE

In order to compare the performance of the iterative (benchmark) and model-based control design, the system response for a mass step and a position step are evaluated on the experimental setup.

5.1 Load mass variation

The load mass variation is performed with the mover stabilized in the desired position of $d_1 = d_2 = 1\,\text{mm}$. A load mass of 1 kg is connected to the mover, yielding an overall mover mass of 1.24 kg. By enabling the EPM control at $t = 100\,\text{ms}$ with the initially switched off EPM, i.e. having zero reluctance force $F_{EPM}(t = 0\,\text{s}) = 0\,\text{N}$, the system response to a mass step of 1.24 kg is evaluated for both EPM control approaches, shown in Fig. 5. Initially, the mover mass is levitated by the LAs, resulting in an offset current of about $i_{off} = 0.84\,\text{A}$.

The iterative control starts to apply current pulses i_{EPM} with linearly increasing peak values until the termination condition is fulfilled ($|i_{off}| < 10\,\text{mA}$). Disturbances of the measured current i_{EPM} are observable, caused by the sampling frequency of the rapid prototyping system and the low-side shunt resistor-based measurement. The analog peak current control ensures the desired peak value, with the visible uncertainty being artefacts of the measurement. After numerous current pulses, the iterative control fulfils the termination condition at 9 s and a stationary state is reached.

The model-based control starts with a peak current of 10 A, which slightly overshoots the desired offset current of 0 A.

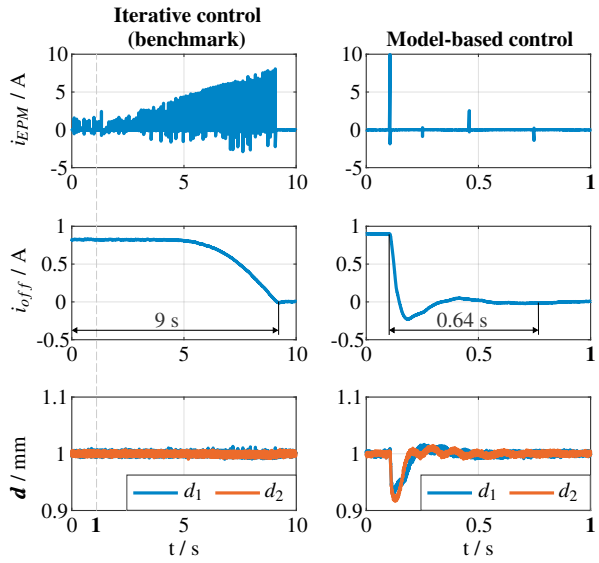

Fig. 5. Experimental system response to a 1.24 kg mass step. At $t = 100$ ms the iterative and the model-based control start to minimize the offset current in the LAs i_{off} with magnetization current pulses i_{EPM} to tune the reluctance force of the EPM (note the adjusted time scale).

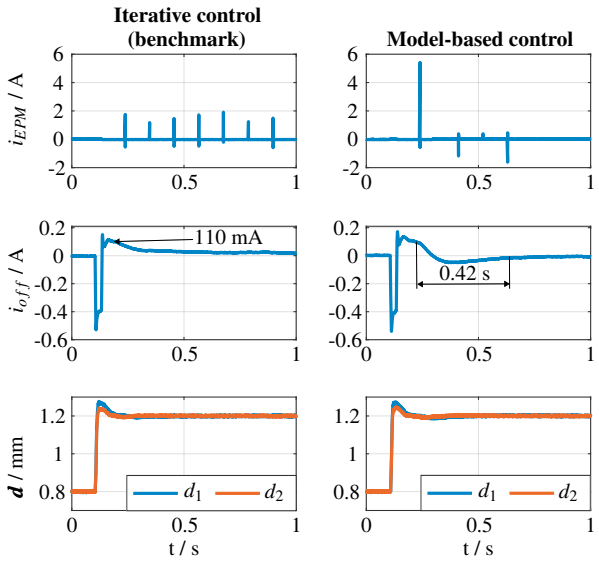

Fig. 6. Experimental system response to a 400 µm reference position step of d_1 and d_2 at $t = 100$ ms. The inner position control loop adapts the mover position, resulting in a changed offset current in the LAs i_{off}. Subsequently, the iterative and model-based control retune the reluctance force of the EPM with magnetization current pulses i_{EPM}.

Subsequently, an increased position error can be observed, caused by the transient disturbance force of the magnetization current pulse. Due to the higher bandwidth of the inner position control, the position error is largely compensated within the EPM control sampling time of 100 ms, having no impact to the response of the model-based control. The model-based control reduces the magnitude of the offset current to less than 10 mA with only four magnetization current pulses over 0.64 s, equalling a factor 14 shorter response time while providing similar accuracy. Calculating the relation between the compensated gravitational force of about $F_G = mg = 12.2$ N and the duration of the compensating process, the tuning rate of the iterative control is determined to 1.35 N/s, whereas the model-based control achieves an improved force tuning rate of 19 N/s. The higher force tuning rate improves the energy efficiency due to the reduced power dissipation in the Lorentz coils and enables the gravity compensation of higher dynamic load mass changes.

5.2 Position tracking

A variable reluctance actuator generates a position-dependent force. If the mover mass remains constant but the mover position is changed, the reluctance force needs to be retuned by the EPM control for maintaining the force equilibrium. Therefore, the mover is loaded with 1 kg and at $t = 100$ ms a reference position step from 0.8 mm to 1.2 mm is applied to each position controller of d_1 and d_2. The subsequent system response is shown in Fig. 6 for both control approaches. Initially, the mover is accelerated towards the position of 1.2 mm, indicated by the negative offset current in both measurements. As the mover position approaches the reference of 1.2 mm, the offset current becomes positive due to the decreased reluctance force caused by the reduced magnetic flux in the air gaps. Both EPM control approaches start to respond to the offset current of about 110 mA after elapsing the sampling time of 100 ms.

The iterative control starts to increase the magnetization current pulses until the the magnitude of the offset current is smaller than 10 mA. However, the offset current does not remain within the borders of the termination condition and the iterative control starts again with a current pulse of 0.1 A. This cyclic response is repeated without fulfilling the termination condition stationary. The disturbance force of the magnetization current pulses attracts the mover and the offset current is reduced without changing the magnetization of the EPM, revealing that the iterative control is not able to stationary reduce the magnitude of the offset current to smaller than 10 mA.

The model-based control design requires four current pulses with the first one overestimating the required tuning current, yielding a negative offset current. Three subsequent negative current pulses reduce the compensating reluctance force to a stationary operating point within 420 ms. In contrast to the iterative control, the model-based control is able to fulfil the termination condition by decreasing the offset current to smaller than 10 mA and no further magnetization current pulses are required. This experiment shows an improved robustness of the model-based control design in comparison to the iterative control, enabling a higher energy efficiency of the gravity compensating mechanism.

In summary, the introduced model-based control design improves the force tuning rate in comparison to the iterative controller [Pechhacker et al. (2022)] by a factor of 14 to 19 N/s and achieves higher robustness in variable mover positions.

6. CONCLUSIONS

A hysteresis model-based flux control to tune the magnetization of a electropermanent magnet is proposed in this paper. The variable magnetic flux of the electropermanent magnet results an adaptable reluctance force, which is used for zero power gravity compensation. Current pulses in the enveloping coil seamlessly tune the magnetization of the electorpermanent magnet. By adapting the reluctance force according to the grav-

itational forces of the loaded mover, a zero power operating point is reached. A non-linear control design is synthesized by approximating the identified hysteresis of the electropermanent magnet and an integrator is added to compensate modelling uncertainties. By comparing the model with measurement results, the modelling of the hysteresis is verified. The control performance is experimentally evaluated for load mass steps and the mover position steps. The introduced model-based control approach increases the force tuning rate by a factor of 14 in comparison to the state of the art iterative control [Pechhacker et al. (2022)]. Additionally, the robustness of the gravity compensation system is improved for variable mover positions. Future work could focus on the inner position control design to ideally compensate the disturbance force of the magnetization current pulse, which may further increase the force tuning rate based on a higher achievable sampling frequency of the outer model-based flux control.

REFERENCES

Campbell, P. and Al-Murshid, S. (1982). A model of anisotropic alnico magnets for field computation. *IEEE Transactions on Magnetics*, vol. 18, no. 3, 898–904.

Chen, S., Huang, K., and Juang, F. (2003). Improvement of a capacitor discharge impulse magnetizer circuit. In *The Fifth International Conference on Power Electronics and Drive Systems, 2003. PEDS.* IEEE.

Choi, Y.M. (2009). A new magnetic bearing using halbach magnet arrays for a magnetic levitation stage. *Review of Scientific Instruments*, vol. 80, no. 4, 045106-1–045106-9.

Deng, R. (2017). *Integrated 6-DoF Lorentz Actuator with Gravity Compensation for Vibration Isolation in In-Line Surface Metrology*. Ph.D. thesis, Delft University of Technology, Delft.

Furlani, E.P. (2001). *Permanent Magnet and Electromechanical Devices: Materials, Analysis, and Applications*. Electromagnetism series. Elsevier BV, San Diego.

Golob, M. and Tovornik, B. (2003). Modeling and control of the magnetic suspension system. *ISA Transactions*, vol. 42, no. 1, 89–100.

Hiemstra, D.B., Parmar, G., and Awtar, S. (2014). Performance tradeoffs posed by moving magnet actuators in flexure-based nanopositioning. *IEEE/ASME Transactions on Mechatronics*, vol. 19, no. 1, 201–212.

Hol, S., Lomonova, E., and Vandenput, A. (2006). Design of a magnetic gravity compensation system. *Precision Engineering*, vol. 30, no. 3, 265–273.

Knaian, A. (2010). *Electropermanent magnetic connectors and actuators: devices and their application in programmable matter*. Ph.D. thesis, Massachusetts Institute of Technology, Dept. of Electrical Engineering and Computer Science, Massachusetts.

Li, Z., Zhang, X., Su, C.Y., and Chai, T. (2015). Nonlinear control of systems preceded by preisach hysteresis description: A prescribed adaptive control approach. *IEEE Transactions on Control Systems Technology*, vol. 24, no. 2, 451–460.

Pechhacker, A., Wertjanz, D., Csencsics, E., and Schitter, G. (2022). Integrated electromagnetic actuator with adaptable zero power gravity compensation (submitted). *IEEE Transactions on Industrial Electronics*.

Qin, S., Zhang, H., Mao, Y., Yang, L., Li, X., Hu, Z., and Cheng, X. (2020). Electropermanent magnet blank holder technique in sheet metal deep drawing. *The International Journal of Advanced Manufacturing Technology*, vol. 106, no. 1, 5497–5507.

Raab, M., Hutter, M., Kazi, A., Schinkoethe, W., and Gundelsweiler, B. (2021). Magnetically levitated linear drive using an active gravity compensation based on hybrid shape memory actuators. *IEEE/ASME Transactions on Mechatronics*, vol. 26, no. 3, 1380–1391.

Rakotondrabe, M. (2012). Classical prandtl-ishlinskii modeling and inverse multiplicative structure to compensate hysteresis in piezoactuators. In *American Control Conference*. IEEE.

Rakotondrabe, M. (2011). Bouc–wen modeling and inverse multiplicative structure to compensate hysteresis nonlinearity in piezoelectric actuators. *IEEE Transactions on Automation Science and Engineering*, vol. 8, no. 2, 428–431.

Schmidt, R.M., Schitter, G., Rankers, A., and van Eijk, J. (2020). *The design of high performance mechatronics : high-tech functionality by multidisciplinary system integration*. Delft University Press, Amsterdam.

Stadler, G., Csencsics, E., Ito, S., and Schitter, G. (2022). High precision hybrid reluctance actuator with integrated orientation independent zero power gravity compensation. *IEEE Transactions on Industrial Electronics*, vol. 69, no. 12, 13296–13304.

Velez, C., Tatum, L.P., Herstein, B.S., Becker, C.P., and Arnold, D.P. (2018). Batch-fabrication and characterization of miniaturized axisymmetric electropermanent magnets. *Journal of Physics: Conference Series*, 1052, 012045.

Wertjanz, D., Csencsics, E., Schlarp, J., and Schitter, G. (2020). Design and control of a MAGLEV platform for positioning in arbitrary orientations. In *2020 IEEE/ASME International Conference on Advanced Intelligent Mechatronics (AIM)*. IEEE.

Wertjanz, D., Kern, T., Pechhacker, A., Csencsics, E., and Schitter, G. (2022). Robotic precision 3D measurements in vibration-prone environments enabled by active six DoF sample-tracking. In *2022 IEEE/ASME International Conference on Advanced Intelligent Mechatronics (AIM)*. IEEE.

Yao, T.F., Duenner, A., and Cullinan, M. (2016). In-line dimensional metrology in nanomanufacturing systems enabled by a passive semiconductor wafer alignment mechanism. *Journal of Micro and Nano-Manufacturing*, vol. 5, no. 1.

Yonnet, J.P. (1981). Permanent magnet bearings and couplings. *IEEE Transactions on Magnetics*, vol. 17, no. 1, 1169–1173.

Zhang, H., Kou, B., Jin, Y., Zhang, H., and Zhang, L. (2014). Research on a low stiffness passive magnetic levitation gravity compensation system with opposite stiffness cancellation. *IEEE Transactions on Magnetics*, vol. 50, no. 11, 1–4.

Zhu, T., Cazzolato, B., Robertson, W.S., and Zander, A. (2015). Vibration isolation using six degree-of-freedom quasi-zero stiffness magnetic levitation. *Journal of Sound and Vibration*, vol. 358, 48–73.